International Journal of Computational Vision and Biomechanics
Vol. 6 No. 1 (January-June, 2020)

Minimal Path Techniques for Automatic Extraction of Microglia Extensions

Youssef Rouchdy[1], Laurent D. Cohen[1], Olivier Pascual[2] and Alain Bessis[2]

[1]*Ceremade, Université Paris Dauphine, 75775 Paris Cedex 16-France*

[2]*Institut de Biologie de l'Ecole Normale Superieure, Inserm 1024-CNRS 8197, 46 rued'Ulm, 75230 Paris Cedex 05, France*

Received: 15th November 2019 Revised: 10th December 2019 Accepted: 19th January 2020

This paper presents new methods to segment thin tree structures, which areforexamplepresent inmicrogliaextensionsand cardiacorneuronal blood vessels. The Fast Marching method allows the segmentation of tree structures from a single point chosen by the user when a priori information is available about the length of the tree. However, in general, there is no way to stop the propagation automatically. In our case, no a priori information about the length of the microglia extensions is available. We propose here to use Harris points to deûne a criterion to stop the propagation. The tree structure is deûned as the set of minimal paths, relatively to the weighted distanceby a costpotential, extractedfrom a sourcepoint(root of the tree) to allHarrispoints.Thesepoints canbe used alsototrack thetree structure in image sequences. Numerical results from synthetic and microscopic images are presented.

Keywords: *Minimalpaths · Fast Marching · Tree structures · Segmentation · Microglia*

1. INTRODUCTION

In this paper we present novel methods for the segmentation of tree structures. These methods are based on minimal paths with a metric designed from the images and can be applied to the segmentation of numerous structures, such as: microglia extensions; neurovascular structures; blood vessel; pulmonary tree. Following our main motivation, we will present applications of our methods to microglia extensions.

Recent developments in imaging such as fluorescent probes and reporters combined to two photon microscopy brought new field of investigation in neuroscience. It now allows researchers to follow in *vivo* dynamic movements of cells in 3D. Such approaches revealed that microglia, a subtype of glial cells, are particularly motile in the Central Nervous System (CNS). Besides their highly mobile processes, microglia are the major inflammatory eector cells of the brain and consequently are involved in most of CNS diseases. Understanding the logic of microglia motility might at term provide an ecient tool to detect early symptoms of diseases such as Alzheimer or multiple lateral sclerosis. Although much work is devoted to the segmentation of vascular trees in medical images, few attempts have been made to extract microglia extensions and were restricted to the main branches ([9], [39]). Since the microglia extensions are very thin, the centerlines of the extensions are enough to characterize the structure and the motion of the microglia. From our experience with vascular trees we can tell that microglia segmentation can be much more difficult, due to very thin branches and noise.

Corresponding author: *E-mail: rouchdy@gmail.com*

While there are few studies dedicated to the segmentation of microglia structures, there is a large number of studies dedicated to the extraction of the vascular or airway trees. For a review of methods used to extract these structures, see [18, 19, 25, 1, 4, 21]. Among the methods used to segment these tree structures we consider the three following models, classified according to the method used to extract the tubular aspect of the tree: centerline based models; surface models; and 4D curve models. The first category focuses on directly extracting the centerlines of the tubular tree [22, 35]. However, after extracting the centerlines a second process can allow to segment the lumen of the tree, see [3]. The second category extracts directly the surface of the vessel. This approach includes explicit and implicit surface models. The former approach uses a parametric representation of the tubular structure [14]. These models are not adapted to the segmentation of complex tree structures while implicit methods can evolve the surface to complex shape changes and handle changes in topology [23, 40]. However, initializations must be performed carefully to get an accurate segmentation.

Minimal paths techniques were extensively used for centerlines extraction of tubular tree structures. These approaches are more robust than the region growing methods, particularly in the presence of local perturbations due to the presence of stenosed branches of the tree or imaging artefacts where the image information might be insucient to guide the growing process. Several minimal path techniques have been proposed to deal with this problem [2, 38, 10]. These techniques consist in designing a metric from the image in such a way that the tubular structures correspond to

geodesic paths according to this metric [7]. Solving the problem from the practical point of view consists of a front propagation from a source point within a vessel, which is faster on the branches of the vascular tree. These methods required the definition by the user of a starting point (propagation source) and end points. Each end point allows to extract a minimal path from this point to the source point, the points located on the minimal path are very likely located on the vessel of interest. Few works have been devoted to reduce the interaction of the user in the segmentation of tree structure to the initialization of the propagation from a single point. Authors of [15] defined a stopping criterion from a medialness measure, the propagation is stopped when the medialness drops below a given threshold. This method might suer from the same problem as the growing region, the medialness might drop below the given threshold in the presence of pathology of imaging artefacts. Wink *et al.* [37] proposed to stop the propagation when the geodesic distance reaches a certain value. However, this method is limited to the segmentation of a single vessel and the definition of the threshold of the geodesic distance is not straightforward. Cohen *et al.* [6] proposed to stop the propagation following a criterion based on some geometric properties of the region covered by the front. In [11], assuming the total length of the tree structure to be visited is given, the stopping criterion is based on the Euclidean length of the minimal path.

Li *et al.* [20] proposed a 4D curve model with a key point searching scheme to extract multi-branch tubular structures. The vascular tree is a set of 4D minimal paths, giving 3D centerlines and width. While this method has the advantage to segment vessel centerlines and surfaces simultaneously, it requires the definition of eight parameters. One point inside the tubular structure and the radius are used to initialize the Fast marching propagation, three parameters are used to set the Fast Marching potential and three distance parameters limit the propagation to the inside of the tubular structure to avoid leakage outside the tree. These last three parameters required an important intervention of the user since they are crucial to extract the whole structure. If these distance parameters are not suitable, parts of the tree structure may be missed during the propagation.

Recently, the Geodesic Voting method [27–29] was proposed to extract tree structures without using any a priori information and based on the user providing only a single point on the tree structure. It consists in computing geodesics from a given source point to a set of end points scattered in the image. The target structure corresponds to image points with a high geodesic density. The geodesic density is defined at each pixel of the image as the number of geodesics that pass over this pixel. Since the potential takes low values on the tree structure, geodesics will locate preferably on this structure and thus the geodesic density should be high.

Here, we present methods to extract tree structures without using any a *priori* information and based on the user providing only a single point on the tree structure. The proposed method is less time consuming than the geodesic voting method, only few minimal paths are needed to segment the target tree. In contrast, the geodesic voting method requires the extraction of a large number of geodesics to define an accurate geodesic density. However, the proposed method is based on the assumption that the extremities of the tree are included in the set of corner points in the images. This assumption is met in many applications such as the microglia extensions, which are the main focus of this paper. The geodesic voting method has a broader application since it does not rely on this assumption.

Some of the main results of the paper were presented in the conference paper [30], we improved here the presentation of the method and evaluate it on a larger data set. We propose to use geometric characteristic of the tree as criterion to stop the propagation: extremities and junctions of the tree. We detect these points as corners by the Harris detector [16]. The tree structure is approximated by the set of minimal paths, relatively to the weighted distance by a cost potential, from the Harris points to the root of the tree. The root point corresponds to the propagation source and is the only information given by the user. Since the potential takes low values on the tree structure, geodesics will locate preferably on this structure. The method was applied to segment Microglia extensions from confocal microscope.

The paper is organized as follows: in Section 2 we give tools needed to present our segmentation method in Section 3; in Section 4 we apply our method to segment microglia extensions from two photon images; in Section 5, we give a conclusion and discuss possible improvements of the method.

2. BACKGROUND

2.1. Minimal Paths

The minimal path theory for the extraction of contours from the image was inspired by the Fermat principle in geometrical optics: the light trajectory $y(s)$ minimizes the optical distance between $x_0 = y(0)$ and $x_1 = y(L)$, where s is the arclength and L is the length of the trajectory which follows the curve $y(s)$ that minimizes the travel time τ:

$$\tau(x_0, x_1) = \int_0^L \frac{ds}{c(y(s))} \tag{1}$$

where propagation speed c is a function depending on the medium of the propagation. In homogeneous media the function c is a constant, the trajectories correspond

to lines. In a medium with two regions, the function c takes two values: c_1 in the first region and c_2 in the second region. The trajectory, in this case, corresponds usually to two joint segments, each segment belonging to one region (satisfying Snell law). We are interested here in the case of a medium with a continuous velocity c, see [7].

In the context of image segmentation Cohen and Kimmel proposed, in [7], a deformable model based on the optical distance (1). The model is formulated as finding a geodesic for a weighted distance:

$$\min_y \int_0^L (w + P(y(s)))ds, \tag{2}$$

the minimum is considered over all curves $y(s)$ traced on the image domain Ω that link the two end points, that is, $y(0) = x_0$ and $y(L) = x_1$. The constant w imposes regularity on the curve. $P > 0$ is a potential cost function computed from the image, it takes lower values near the edges or the features. For instance $P(y(s)) = I(y(s))$ leads to darker lines while $P(y(s)) = g(\|\nabla I\|)$ leads to edges, where I is the image and g is a decreasing function.

To compute the solution associated to the source x_0 of this problem, [7] proposed a Hamiltonian approach: Find the geodesic weighted distance U to x_0 that solves the eikonal equation

$$\|\nabla U(x)\| = w + P(x) \ \forall x \in \Omega \tag{3}$$

The ray y is subsequently computed by back-propagation from x_1 by solving the ordinary differential equation (ODE)

$$y'(s) = -\nabla U(y). \tag{4}$$

Fig. 1 shows a simple example of minimal path on a synthetic image.

The only stable schemes that solve the eikonal equation compute the viscosity solution [8]. The first work that uses the viscosity solution for this kind of problems is from Vidale [36]. An iterative numerical scheme to solve eikonal equation was proposed in [31, 12]. In such iterative scheme, at least complexity $O(mn^2)$ is needed, where n is the total number of grid points and m is the number of iterations that permit an estimation of the solution. In the next section, we present the Fast Marching algorithm introduced in [33] to solve this problem in complexity $O(n \log(n))$. Some other schemes based on different tricks can lead to $O(n)$.

2.2. Fast Marching Method

The idea behind the Fast Marching algorithm is to propagate the wave in only one diffrection, starting with the smallest values of the action map U and progressing to the largest values using the upwind property of the scheme. Therefore, the Fast Marching method permits only one pass on the image starting from the sources (where $U = 0$) in the upwind direction. We briefly recall the principle of the Fast Marching method, for details see [33, 34, 5]. The grid points are partitioned into three dynamic sets: trial points, alive points and far points. Alive points are the grid points for which a value U has been computed and will not be changed any more, while Far points are those for which there is no possible estimate of U yet. Trial points are points that are not alive, and that have at least one neighbor that is alive, in order to get an estimate of U from the discrete version of Equation (3). The trial points correspond to a dynamic boundary that separates far points and alive points. At each step, the trial point with the minimum value of the action map U is moved to the set of alive points. To reduce the computing time, the trial points are stocked in a data structure referred to as min-heap (the construction of this data structure is described in [33, 34]). The complexity to change the value of one element of the min-heap is $O(\log(n))$. Hence, the total complexity for Fast Marching to reach the n grid points as alive is $O(n \log(n))$. The Dijkstra algorithm, which is also used to find a minimal cost path on a graph, has the same complexity as the Fast Marching algorithm. However, the Dijkstra algorithm leads to metrication error and is not consistent, contrary to the Fast Marching algorithm which converges toward the unique viscosity solution (see [5]). Fig. 1 shows an example of distance map computed with the Fast Marching on a synthetic image.

2.3. Detection of Points of Interest

Characteristic points have been proven successful in solving many vision problems for a long time such as tracking [17] or reconstruction [13], and are more efficient in some applications than other geometric primitives such as edges or segments. One of the most popular detector of corner points is the Harris detector, which is better or equivalent to the other detectors [32]. This comparison is achieved in terms of repeatability: is the point detected in the first image also accurately detected in the second image. Detectors with a good repeatability rate may be useful to understand the motility of the microglia extensions over time. In this work, we focus on the use of such points to segment the microglia extensions.

The Harris detector [16] is based on the Moravec detector [24], which determines the average changes of image intensity that result from shifting a local window in the image by small variations in various directions. The intensity change E produced by the shift (p, q) is :

$$E(p,q) = \sum_{i,j} w_{i,j} \, | I(i+p, j+q) - I(i,j) |^2 \tag{5}$$

where w specifies the image window. We consider here a smooth Gaussian circular window.

The Moravec detector of corners looks for local maxima of E. The Harris detector computes and compares the eigenvalues of the Taylor expansion of E. By using the Taylor formula with small shift, the variation E can be written as:

$$E(p, q) = (p, q)M(p, q)' \quad (6)$$

where M is defined by

$$M\begin{pmatrix} A & C \\ C & B \end{pmatrix},$$

and

$$A = \left(\frac{\partial I}{\partial x}\right)^2 \otimes w, \quad B = \left(\frac{\partial I}{\partial y}\right)^2 \otimes w, \text{ and } C = \frac{\partial I}{\partial x}\frac{\partial I}{\partial y} \otimes w,$$

where $\otimes$ denotes the discrete convolution.

The eigenvalues λ_1 and λ_2 of M correspond to the principal curvatures of E. The corners are characterized by two large eigenvalues λ_1 and λ_2. Note that it is not necessary to compute λ_1 and λ_2, indeed

$$\mathrm{Tr}(M) = \lambda_1 + \lambda_2 = A + B \quad (7)$$

$$\mathrm{Det}(M) = \lambda_1 \lambda_2 = AB - C^2 \quad (8)$$

The corner measure is defined by

$$R = \mathrm{Det}(M) - kTr^2(M), \quad (9)$$

and it is positive in the corner region, negative at the edges and small in the homogenous regions, the parameter k is selected empirically between 0.04 and 0.06. Fig. 1 shows an example of the corner measure R.

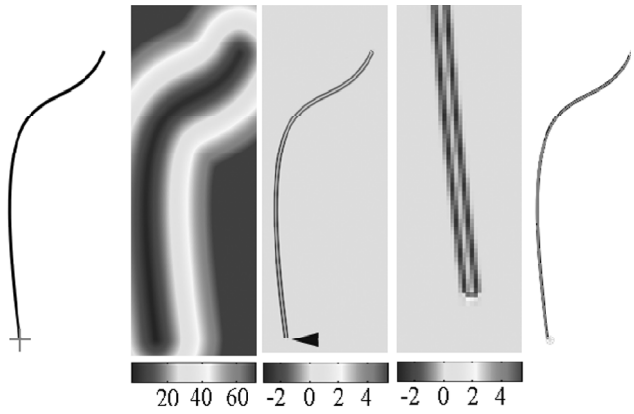

Figure 1: Illustration: Minimal paths and Harris points. First panel: the synthetic image, the red cross corresponds to the source point. Second panel: the distance map computed with the Fast Marching method. Third panel: the corner measure matrix *R* (given by Equation (9)). Fourth panel: zoom on the region indicated by the head-arrow in the third panel. Fifth panel: in green the Harris points detected, the Harris point on the bottom corresponds also to the source point used for the Fast Marching propagation. The red line corresponds to the minimal path between the Harris point on the top and the source point

3. EXTRACTION OF TREE STRUCTURES BY FAST MARCHING AND CHARACTERISTIC POINTS

The Fast Marching method allows us to extract the minimal path between two points. Here, the aim is to extract a tree with minimal intervention by the user. When a priori information about the geometry or the length of the contour to be extracted is available, Cohen and al. proposed in [6] a method to extract a tree structure from one point selected by the user. In the following sections, methods are proposed for the segmentation of tree structures from only one given point without any other a priori information. The method is based on corner points, which are computed by the Harris detector described in section 2.3. A pyramidal approach is used to reduce erroneous detection.

Table 1
Algorithm for the Propagation from the Root wtih Harris Points

Notations:

– x_0 is a starting point located at the root of the tree structure;
– U is the action map.

Initialization:

– detect the Harris points h_i present in the image and choose the root x_0 among them;
– initialize the front propagation, by setting $U(x_0) = 0$.

Loop: proceed according to the Fast Marching algorithm 2.2, updating action maps and min-heap data.

Segmentation: Extract the paths between each Harris point and the root.

Within the image, a set of Harris points are detected. We defined the root of the tree as a point selected by the user from the Harris points. This point can be also defined as the nearest point in the tree to the center of mass of all Harris points. From the root, a front is propagated with the Fast Marching method. For each Harris point that is not the root, a path to the root is extracted by back-propagation. The algorithm is given in the Table 1. Fig. 2 shows that the algorithm is able to extract a tree structure correctly from a noisy synthetic image. This synthetic image is created by using an additive Gaussian noise with zero mean and 0.1 variance to a binary image of a tree structure.

Since there may be Harris points detected that may be due to noise, or to small isolated parts in the image, we have to filter the set of paths and remove some paths that do not correspond to tubular shape. A simple way to do that is to estimate if the potential function is small enough along all paths. In the second step, for all minimal paths extracted from the selected Harris points to the source point using the algorithm given in Table 1, we compute the following measurement:

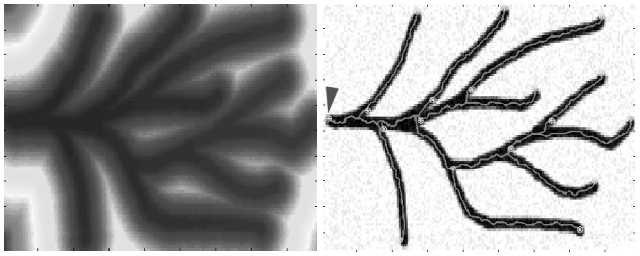

Figure 2: Segmentation results obtained with algorithm 1. Left : the action map from the root seed point; right : the extracted tree, the green circles correspond to the Harris points and the red lines trace the paths from the Harris points to the root of the tree (indicated by the head-arrow)

$$\Gamma(\gamma) = \frac{1}{Le(\gamma)} \int P(\gamma(s))ds \qquad (10)$$

where P is the potential computed from the image; $Le(\gamma)$ is the euclidean length of the path γ. We keep only the minimal paths that have a measure Γ inferior to a given threshold.

4. SEGMENTATION OF MICROGLIA EXTENSIONS FROM CONFOCAL MICROSCOPE IMAGES

The confocal images were composed of a set of 4D (3D+time) image sequences. For each time point, a series of 23 images perpendicular to the *z* axis was acquired, thereby covering the three dimensions of the cell. In this study, segmentation was restricted to static 2D images, e.g. only one time point and only one image from the image series acquired at this time was considered. The microglia images contained much noise. Therefore, we have added two postprocessing steps to get an optimal segmentation: (1) Harris point improvement and (2) minimal path selection. In the first step, a pyramidal approach was used to detect the Harris points in the image. Only the Harris points that appeared in both the first pyramid (original image, see Fig. 3, center panel) and in the second pyramid (see Fig. 3, right panel, half the resolution of the original image) were used. Some of the erroneous detections were eliminated in this way. In the second step, for all minimal paths extracted from the selected Harris points to the source point, we keep only the minimal paths that have a measure Γ (given by the equation (10)) inferior to a given threshold. Here we choose the potential $P = I^7$, where I is the intensity value of the acquired image.

Fig. 4 and Fig. 5, center column, show the segmentation results with the algorithm given in Table 1. Fig. 4 and Fig. 5, right column, show in green the segmentation results obtained by selecting the minimal paths that have the measure Γ inferior to a fixed threshold. Note that a small threshold may lead to the detection of false branches and a large threshold leads to missing branches of the tree. Here, the threshold was defined from the first and the second images and were used to segment a data set of 24 image acquired at different times, see Table 2. The manual correction of the segmentation was performed by a biologist with expertise in microglia motility using the (3D + time) data to tract each extension across slices and time. The center of the cell, which corresponds to the root of the propagation, was chosen manually in the first image. The segmentation results are satisfying. Note that some parts of the tree were not

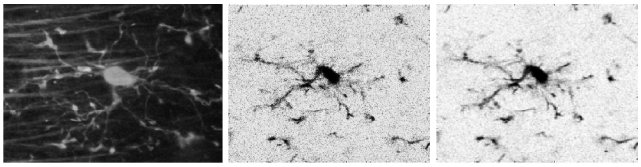

Figure 3: Confocal microscope images of a microglia. Left panel: a projection of 23 slices. The green structures correspond to the microglia and neuronal extensions are red. Center panel: a single image from a series of images perpendicular to the z axis, showing the microglia. Right panel: a second stage of the pyramid of the image shown in the center panel (half of the resolution of the original image). This image was used to compute the Harris points

Table 2
Comparison of Our Segmentations (Algorithm) with the Manual Segmentations on 24 Microglia Images

Microglia	*Manual*	*Algorithm*	*Undetected*	*False detection*
Image #01	33	29	06	02
Image #02	35	34	04	03
Image #03	31	30	03	02
Image #04	26	24	06	04
Image #05	31	31	04	04
Image #06	32	29	05	02
Image #07	24	22	07	05
Image #08	30	24	07	01
Image #09	28	27	04	03
Image #10	20	20	03	03
Image #11	21	17	04	00
Image #12	28	24	07	03
Image #13	19	17	03	01
Image #14	26	21	05	00
Image #15	20	18	03	01
Image #16	21	17	04	00
Image #17	20	18	03	01
Image #18	22	16	06	00
Image #19	23	18	07	02
Image #20	26	18	08	00
Image #21	25	21	06	02
Image #22	18	18	03	03
Image #23	22	20	03	01
Image #24	25	21	06	02
Mean	25.25	22.25	04.88	01.88
Std	04.87	05.21	01.65	01.42

present in the studied image, but could be found in the other 22 images of the image series. Hence, some segments of the tree extracted in the 2D segmentation do not correspond to a real contour present (which was corrected manually by the expert in red, see Fig. 4 and Fig. 5, right column). An extension of the proposed methods to the 3D segmentation should solve this problem. Temporal constraints may help to improve partially the segmentation since the microglia motility is still not fully understood and undergoing active research in the biology community. In Fig. 6 we compare our approach with the level set method. This figure illustrates the limitation of the level set method to segment thin tree structure from noisy data as the microglia extensions.

5. DISCUSSION AND CONCLUSION

In this paper, methods for the segmentation of tree structures were proposed, only the selection of one point by the user is required. The main contribution is the use of Harris points to guide the segmentation process. We evaluated our method on 24 datasets, the results are very satisfying in terms of rapidity of analysis and coherence with the manual segmentation of the microglia extensions.

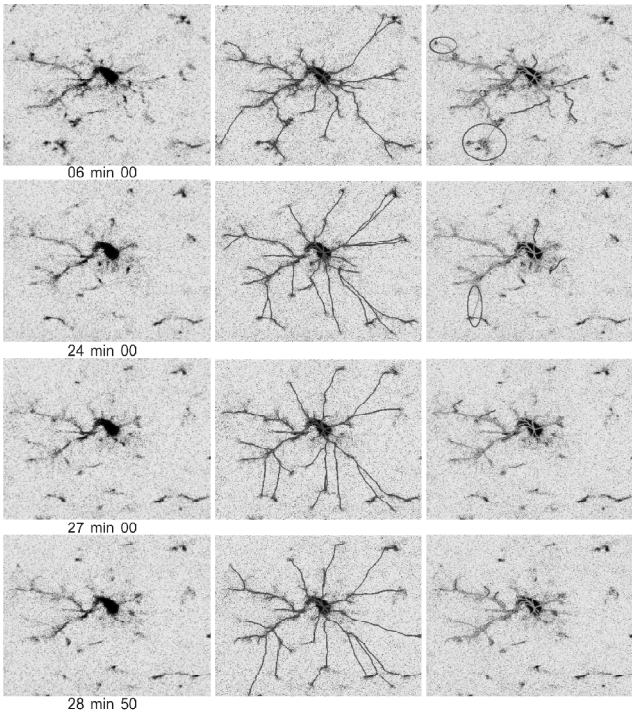

Figure 4: Segmentation of a microglia from confocal microscope images. Left column: microglia images (1 image / 90 seconds); center column: extracted tree structure, the green circles are the Harris points, the red lines trace the paths from the Harris point to the root. The root corresponds to the cell center. Right column: in green the extracted tree structure using the measure (10), red paths show missing branches added by the expert, red ellipses show false detections corrected by the expert.

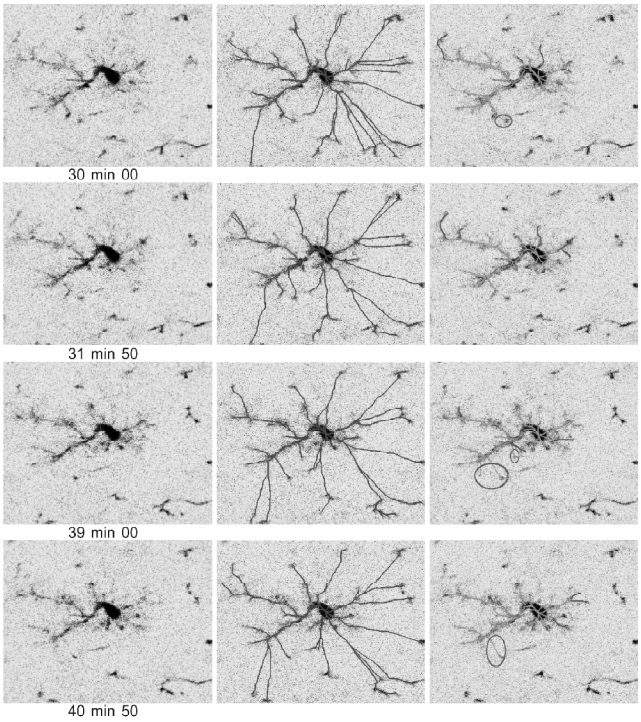

Figure 5: Segmentation of a microglia from confocal microscope images. Left column: microglia images (1 image / 90 seconds); center column: extracted tree structure, the green circles are the Harris points, the red lines trace the paths from the Harris point to the root. The root corresponds to the cell center. Right column: in green the extracted tree structure using the measure (10), red paths show missing branches added by the expert, red ellipses show false detections corrected by the expert

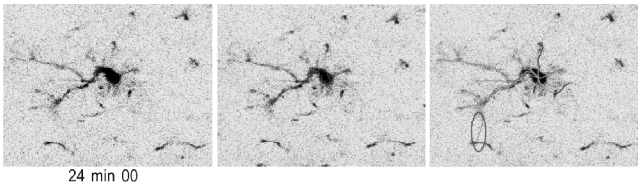

Figure 6: Comparison of the level set method with our approach. Left panel: microglia image; center panel: in red the segmentation result obtained with the level set method. The root corresponds to the cell center. Right panel: in green the extracted tree structure using the measure (10), red paths show missing branches added by the expert, red ellipses show false detections corrected by the expert

In the following we present some extensions and improvements of the proposed method. The microglia is a 3D tree structure and some extensions of the microglia can appear in dierent slices as mentioned in the previous section. The segmentation of the microglia in 3D will allow to track the microglia extensions in dierent slices and therefore allow to extract accurately all the extensions of the microglia. However, the 3D implementation of the method should take into account the anisotropy of the data -e.g-high resolution in the plane of the slice and lower resolution in the perpendicular direction. In this

paper we limit the segmentation to segment only one cell by giving a source on the body of the cell. The acquisition of the images was performed in such a way that the image includes only one cell. The biologists we collaborated with were interested in having to give only one source point for each cell. They thus suggested us to work on a region that includes only one tree structure. However, an extension of the proposed method to segment microglia extensions on images with several microglia cells is desirable. When a direct separation of all tree structure is not obvious manually, the method may be adapted to segment images that contain several disconnected trees by using the appropriate source point for each tree structure present in the image. The user would provide a source point for each tree structure (cell) present in the image. Then, a set of Harris points would be aected to the correspondent source point. Each set of Harris points with the associated source point would allow to segment one cell. The association between a set of Harris points and a source point could be done by using a geodesic distance as criterion to make this partition. The last improvement would be to introduce temporal constraints in the tracking of the microglia extensions over time. The tracking process presented in this paper is realized by successive segmentations at each time point: there are no temporal constraints between the localization of the microglia extensions at dierent acquisition time points. Temporal constraints taking into account the localization of the microglia extensions at previous time may help to constraint the segmentation of the microglia extensions in the following images. For example we can correlate the Harris points detected at dierent time points by using a Kalman filter [26]. This will allow a global consistency between the extracted extensions of the microglia and therefore decrease the number of false detections and undetected extensions.

REFERENCES

[1] Agam, G., III, S.G.A., Wu, C.: Vessel tree reconstruction in thoracic CT scans with application to nodule detection. *IEEE Trans. Med. Imaging* **24**(4), 486–499, (2005).

[2] Avants, B. B., Williams, J. P.: An adaptive minimal path generation technique for vessel tracking in CTA CE-MRA volume images. In: MICCAI '00: Proceedings of the Third International Conference on Medical Image Computing and Computer-Assisted Intervention, pp. 707–716. Springer-Verlag, London, UK (2000).

[3] Bouix, S., Siddiqi, K., Tannenbaum, A.: Flux driven automatic centerline extraction. *Medical Image Analysis* **9**(3), 209–221 (2005).

[4] Carrillo, J., Hern´andez Hoyos, M., Davila-Serrano, E., Orkisz, M.: Recursive tracking of vascular tree axes in 3D medical images. *Int. J. Comput Assisted Radiol Surg* **1**(6), 331–339 (2007).

[5] Cohen, L.: Minimal paths and fast marching methods for image analysis. In: Handbook of mathematical models in computer vision, pp. 97–111. Springer, New York (2006).

[6] Cohen, L.D., Deschamps, T.: Segmentation of 3D tubular objects with adaptive front propagation and minimal tree extraction for 3D medical imaging. *Math. Models Methods Appl. Sci.* **10**(4), 289–305, (2007).

[7] Cohen, L. D., Kimmel, R.: Global minimum for active contour models: A minimal path approach. *International Journal of Computer Vision* **24**(1), 57–78, (1997).

[8] Crandall, M. G., Lions, P. L.: Viscosity solutions of Hamilton-Jacobi equations. *Trans. Amer. Math. Soc.* **277**(1), 1–42, (1983).

[9] Davalos, D., Grutzendler, J., Yang, G., Kim, J., Zuo, Y., Jung, S., Littman, D. R., Dustin, M. L., Gan, W. B.: ATP mediates rapid microglial response to local brain injury in vivo. *Nature Neuroscience* **8**(6), 752–758, (2005).

[10] Deschamps, T., Cohen, L. D.: Minimal paths in 3D images and application to virtual endoscopy. In: Sixth European Conference on Computer Vision, Dublin, Ireland, *ECCV*(2), 543–557, (2000).

[11] Deschamps, T., Cohen, L.D.: Fast extraction of minimal paths in 3D images and applications to virtual endoscopy. *Medical Image Analysis* **5**(4), 281–299, (2001).

[12] Fatemi, E., Engquist, B., Osher, S.: Numerical solution of the high frequency asymptotic expansion for the scalar wave equation. *J. Comput. Phys.* **120**(1), 145–155, (1995).

[13] Faugeras, O., Luong, Q.T.: The geometry of multiple images. MIT Press, Cambridge, MA (2001). The laws that govern the formation of multiple images of a scene and some of their applications, With contributions from Th´eo Papadopoulos.

[14] Frangi, A. F., Niessen,W. J., Hoogeveen, R. M., vanWalsum, T., Viergever, M. A.: Modelbased quantitation of 3D magnetic resonance angiographic images. *IEEE Trans. Med. Imaging* **18**(10), 946–956, (1999).

[15] Gülsün, M. A., Tek, H.: Robust vessel tree modeling. In: International Conference on Medical Image Computing and Computer-Assisted Intervention (MICCAI) (1), pp. 602–611, (2008).

[16] Harris, C., Stephens, M.: A combined corner and edge detection. In: Proceedings of The Fourth Alvey Vision Conference, pp. 147–151, (1988).

[17] Kermad, C., Collewet, C.: Improving feature tracking by robust points of interest selection. In: Vision Modeling and Visualization Conference(VMV), pp. 415–422. Stuttgart, Germany (2001).

[18] Kirbas, C., Quek, F.: A review of vessel extraction techniques and algorithms. *ACM Comput. Surv.* **36**(2), 81–121, (2004).

[19] Lesage, D., Angelini, E. D., Bloch, I., Funka-Lea, G.: A review of 3D vessel lumen segmentation techniques: Models, features and extraction schemes. *Medical Image Analysis* **13**(6), 819–845, (2009).

[20] Li, H., Yezzi, A. J., Cohen, L. D.: 3D multi-branch tubular surface and centerline extraction with 4D iterative key points. In: International Conference on Medical Image Computing and Computer-Assisted Intervention (MICCAI) (1), pp. 1042–1050, (2009).

[21] Lo, P., Sporring, J., Ashraf, H., Pedersen, J. J. H., de Bruijne, M.: Vessel-guided airway tree segmentation: A voxel classification approach. *Medical Image Analysis* **14**(4), 527–538, (2010).

[22] Lorigo, L., Faugeras, O., Grimson, W., Keriven, R., Kikinis,\ R., Nabavi, A., Westin, C. F.: Curves: Curve evolution for vessel segmentation. *Medical Image Analysis* **5**, 195–206, (2001).

[23] Manniesing, R., Velthuis, B. K., van Leeuwen, M. S., van der Schaaf, I. C., van Laar, P. J., Niessen, W. J.: Level set based cerebral vasculature segmentation and diameter quantification in CT angiography. *Medical Image Analysis* **10**(2), 200–214, (2006).

[24] Moravec, H.: Obstacle avoidance and navigation in the real world by a seeing robot rover. In: Robotics Institute, Carnegie Mellon University and doctoral dissertation, Stanford University. tech. report CMU-RI-TR-80-03 (1980).

[25] Mori, K., Hasegawa, J., Toriwaki, J., Anno, H., Katada, K.: Recognition of bronchus in three-dimensional X-ray CT images with application to virtualized bronchoscopy system. Pattern Recognition, International Conference on **3**, 528, (1996).

[26] Rouchdy, Y.: An articulated model with a kalman filter for real time visual tracking. application to the tracking of pedestrians with a monocular camera. In: International Conference on Computer Vision Theory and Applications (VISAPP). Funchal (2008).

[27] Rouchdy, Y., Cohen, L. D.: Image segmentation by geodesic voting. application to the extraction of tree structures from confocal microscope images. In: The 19th International Conference on Pattern Recognition, pp. 1–5. Tampa, Florida (2008).

[28] Rouchdy, Y., Cohen, L.D.: The shading zone problem in geodesic voting and its solutions for the segmentation of tree structures. application to the segmentation of microglia extensions. In: MMBIA 2009: IEEE Computer Society Workshop on Mathematical Methods in Biomedical Image Analysis in conjunction with CVPR'09, pp. 66–71. Los Alamitos, CA, USA (2009).

[29] Rouchdy, Y., Cohen, L. D.: A geodesic voting method for the segmentation of tubular tree and centerlines. In: Eigth IEEE International Symposium on Biomedical Imaging (ISBI'11), pp. 979–983. Chicago, Illinois, USA (2011).

[30] Rouchdy, Y., Cohen, L. D., Pascual, O., Bessis, A.: Segmentation of microglia from confocal microscope images combining the fast marching method with Harris points. In: Microscopic Image Analysis with Applications in Biology, Third International Conference on Medical Image Computing and Computer-Assisted Intervention(MICCAI) Workshop, pp. 1–5. New York, NY (2008).

[31] Rouy, E.: Numerical approximation of viscosity solutions of first-order Hamilton-Jacobi equations with Neumann type boundary conditions. Math. *Models Methods Appl. Sci.* **2**(3), 357–374, (1992).

[32] Schmid, C., Mohr, R., Bauckhage, C.: Evaluation of interest point detectors. *International Journal of Computer Vision* **37**(2), 151–172, (2000).

[33] Sethian, J. A.: A fast marching level set method for monotonically advancing fronts. In: *Proc. Nat. Acad. Sci.*, pp. 1591–1595, (1996).

[34] Sethian, J.A.: Level set methods and fast marching methods, Cambridge Monographs on Applied and Computational Mathematics, vol. 3, second edn. Cambridge University Press, Cambridge (1999).

[35] Swift, R. D., Kiraly, A. P., Sherbondy, A. J., Austin, A. L., Homan, E. A., McLennan, G., Higgins, W. E.: Automatic axis generation for virtual bronchoscopic assessment of major airway obstructions. *Computerized Medical Imaging and Graphics* **26**(2), 103–118, (2002).

[36] Vidale, J.: Finite-dierence calculation of traveltime. B. *Seismol. Soc. Am.* **78**, 2062–2076, (1988).

[37] Wink, O., Niessen, W. J., Verdonck, B., Viergever, M. A.: Vessel axis determination using wave front propagation analysis. In: MICCAI '01: Proceedings of the 4th International Conference on Medical Image Computing and Computer-Assisted Intervention, pp. 845–853. Springer-Verlag, London, UK (2001).

[38] Wink, O., Niessen, W. J., Viergever, M. A.: Minimum cost path determination using a simple heuristic function. *Pattern Recognition, International Conference on* **3**, 7010, (2000).

[39] Wu, L. J., Zhuo, M.: Resting microglial motility is independent of synaptic plasticity in mammalian brain. *J. Neurophysiol* **99**, 2026–2032, (2008).

[40] Yan, P., Kassim, A. A.: Segmentation of volumetric MRA images by using capillary active contour. *Medical Image Analysis* **10**(3), 317–329, (2006).